Available online at www.sciencedirect.com
SCIENCE DIRECT®
Journal of Non-Crystalline Solids 332 (2003) 166–172
JOURNAL OF NON-CRYSTALLINE SOLIDS
www.elsevier.com/locate/jnoncrysol

Liquid–liquid phase separation in alkali-borosilicate glass. An impedance spectroscopy study

M.O. Prado *, A.A. Campos Jr., P.C. Soares, A.C.M. Rodrigues, E.D. Zanotto

LaMaV – Vitreous Materials Laboratory, Department of Materials Engineering, Federal University of São Carlos – UFSCar, CEP 13.565-905, São Carlos SP, Brazil

Received 19 March 2003

Abstract

We followed the first stages of liquid–liquid phase separation in an alkali-borosilicate glass by complex impedance spectroscopy at constant temperatures below and above the glass transition temperature, T_g. We found a new feature of the electrical conductivity behavior: at temperatures below T_g, the electrical conductivity, σ, diminished with time, while above T_g, the electrical conductivity increased. The activation energy, E_a, for electrical conductivity was largest for samples heat-treated below T_g. Other techniques, such as simultaneous small angle X-ray scattering (SAXS), wide angle X-ray scattering (WAXS), and transmission electron microscopy (TEM) were also used. After annealing the glass inside the immiscibility gap, TEM shows a structure with a few Angstroms in size. Above and below the glass transition temperature, in situ SAXS isothermal experiments show an increase of the scattered intensity with time, while WAXS confirms that no crystallization occurred. These facts suggest that glass heat treated below T_g develops a SiO_2 rich matrix with lower electrical conductivity and isolated sodium- rich regions. Annealing above T_g (of the quenched glass) seems to produce an interconnected Na-rich phase, which dominates the electrical conductivity.

1. Introduction

Liquid–liquid phase separation (PS) kinetics and morphology of borosilicate glasses have been thoroughly studied by several techniques [1–3], but only few works using impedance spectroscopy are dedicated to this subject. For example, Ravagnani et al. [4] determined by this technique the critical temperature under which a sodium borosilicate glass is phase-separated. PS was also evidenced by impedance spectroscopy in a polycrystalline $La_{0.3}Pr_{0.4}Ca_{0.3}MnO_3$ manganite [5].

In this paper we use complex impedance spectroscopy to follow PS during isothermal heat treatments below and above the glass transition temperature, T_g, of the homogeneous glass (before PS), and make an attempt to correlate the electrical behavior with structural changes.

Borosilicate glasses are model glasses to study the kinetics of transformation due to their high viscosity. Thus, for certain compositions and cooling path, PS free samples can be produced by

* Corresponding author. Present address: Comisión Nacional de Energía Atómica-Centro, Atómico Bariloche (8400), San Carlos de Bariloche (RN), Argentina. Tel.: +54-2944 445230; fax: +54-2944 445299.

E-mail address: pradom@cab.cnea.gov.ar (M.O. Prado).

0022-3093/$ - see front matter © 2003 Elsevier B.V. All rights reserved.
doi:10.1016/j.jnoncrysol.2003.09.031

splat cooling. Moreover, when applied to the study of PS kinetics, impedance spectroscopy has some advantages, in comparison, for example, to direct transmission electron microscopy (TEM) observation such as: (i) negligible energy is dissipated in the sample by the technique, thus one can easily control the sample temperature by simple putting it in a furnace; and (ii) the electrical conductivity is very sensitive to the glass structure and composition.

This work covers the following aspects: (a) the chosen material is an important alkali-borosilicate glass, candidate for nuclear wastes immobilization [6,7] and PS can deteriorate its corrosion resistance; (b) the main technique used here for the study of the PS kinetics is impedance spectroscopy, but small angle X-ray scattering (SAXS), wide angle X-ray scattering (WAXS) and TEM data are also presented; (c) PS kinetics below T_g is also investigated; (d) the information gathered allows one to propose which structural changes take place during PS; (e) we confirmed by SAXS that vitreous phases having different electronic density develop during annealing above and below T_g. Simultaneous WAXS ruled out concurrent crystallization.

2. Experimental methods

2.1. Glass preparation

We investigated an alkali-alumino-borosilicate glass with the following composition: SiO_2: 71.7, B_2O_3: 8.33, $A1_2O_3$: 8.56, MgO: 1.00, CaO: 2.67, Na_2O: 7.44 wt% that is of interest for nuclear waste immobilization [6]. The glass was melted for 2 h at 1600 °C. Samples were prepared by splat cooling a liquid between two stainless steel plates at room temperature. This procedure allowed us to minimize bubbles, and PS during cooling. Transparent, colorless, few millimeters thick specimens were then obtained.

2.2. Impedance spectroscopy

Impedance measurements were made on 2 mm thick, 1×1 cm^2 flat samples. Both sides were polished with 0.5 μm cerium oxide. Platinum electrodes were deposited by sputtering on both sample faces as electrical contacts for impedance measurements. Measurements were made with a computer controlled HP 4192 LA impedance meter. This equipment allows the frequency f to be varied from 5 to 13×10^6 Hz, and can measure impedances up to 6 MΩ.

Complex impedance data may be represented in several correlated formalisms, such as impedance Z vs. f, admittance Y vs. f, or the Bode plots [8]. However, for poor conductors, the Nyquist plot (the opposite of the imaginary part of impedance ($-\mathrm{Im}(Z)$) at the y-axis, and the real part $\mathrm{Re}(Z)$ in the x axis) is the most frequently employed representation. In a Nyquist plot (Fig. 1) the material's

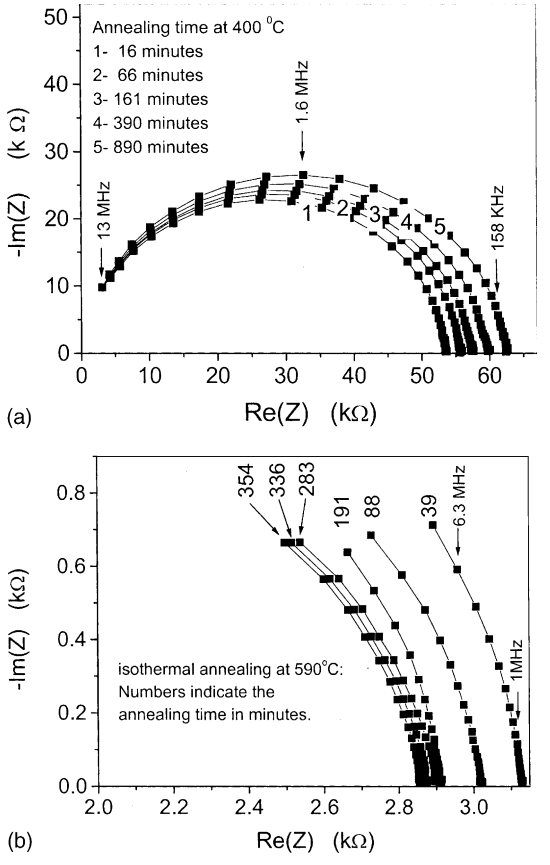

Fig. 1. (a) Sequential Nyquist diagrams obtained during annealing a splat cooled sample at 400 °C; (b) sequential Nyquist diagrams obtained during annealing a splat cooled sample at 590 °C.

resistance, R, is read at the low frequency intersection of the semi-circle with the x-axis.

2.2.1. Electrical conductivity changes during liquid–liquid phase separation

The PS kinetics was followed with impedance spectroscopy measurements at 400, 510, 550, 575, 590, 600, and 690 °C. The glass transition temperature, $T_g = 580$ °C, of the splat cooled glass was measured by differential scanning calorimetry. From SAXS experiments the immiscibility temperature, T_{im}, was estimated to be above 725 °C. For each kinetic measurement, the furnace was first stabilized at the annealing temperature, then the sample was introduced in the furnace producing a temperature decrease of a few degrees. After a few minutes, the equilibrium temperature was recovered and sequential impedance spectra were taken at convenient time intervals during several hours.

For each temperature, a set of spectra was obtained. At each time, the electrical conductivity, σ, was determined using the relation $\sigma = (1/R) \times (I/A)$, where R is the sample resistance read at the low frequency intersection of the semicircle at the Nyquist diagram, A is the samples' electrode area and I its length or thickness. $\sigma(t)$ vs. time plots were then constructed.

2.2.2. Activation energy of the heat treated samples

The evolution of the electrical conductivity was measured at each one of the temperatures listed above. After an initial high rate of the electrical conductivity change, slow rates were observed. At this time, although the equilibrium PS structure had not been reached (in that case σ should not vary with time), and would require annealing times larger than the laboratory time scale, we expect that the reached structure was characteristic of the heat treatment temperature. Then, when the rate of σ change was well below the initial rate, the samples were quenched into air at room temperature to retain the PS structure (frozen structure) correspondent to the annealing temperature for further measurements.

To characterize each frozen structure, the corresponding activation energy for electrical conductivity, E_a, was measured in a temperature range well below the annealing temperature employed at the isothermal investigation of electrical conductivity. Each E_a was taken from Arrhenius plots of $\log(\sigma)$ vs. $1/T$. A plot of E_a vs. annealing temperature was drawn to show the dependence of E_a with the sample's structure (or with the annealing temperature).

2.3. SAXS measurements and data analysis

For SAXS and WAXS measurements, thin glass layers of about 150 μm thick were prepared by grinding and polishing glass slices with 0.5 μm cerium oxide, which proved to have the adequate attenuation for the 7.7 KeV X-ray beam used in the experiments.

Two glass samples were characterized using simultaneous SAXS–WAXS: at 690 and 560 °C during in situ PS ($T_g = 580$ °C). These measurements were performed at the National Synchrotron Light Laboratory (LNLS), Brazil.

WAXS was used to confirm that no devitrification occurred during the experiment.

SAXS was used to determine if phases with different electronic density precipitated during the annealing process. When a two phase sample having an electronic density difference $\Delta\rho$ is illuminated with X-rays, a diffracted intensity $I(q)$ as a function of the dispersed radiation momentum, q, is obtained, which is proportional to $\Delta\rho^2$, the volume V of the particles squared and the number N of particles, as shown by Eq. (1):

$$I(q) \propto \Delta\rho^2 V^2 N f(q, \Lambda), \tag{1}$$

where $f(q, \Lambda)$ is a function which depends upon the shape of the particles, through the adimensional factor Λ [9].

Synchrotron light with $\lambda = 1.608$ Å was used at a sample-detector distance = 571.03 mm, which allowed the measurement of dispersed radiation from $q = 0.01$ A^{-1} (q_{min}) up to $q = 0.5$ A^{-1} (q_{max}). The general experimental setup is described in Ref. [10].

Each SAXS curve was corrected for standard instrumental factors, as well as for sample attenuation. The curve measured at time = 0 was subtracted from all the following curves in order to show the evolution of the scattered intensity with

time. The sequential measured spectra were analyzed.

SAXS curves were measured during several hours at 5 or 10 min intervals. The evolution of the Porod invariant Q with time was calculated using Eq. (2).

$$Q = \int_0^\infty I(q)q^2 d. \tag{2}$$

2.4. Transmission electron microscopy

Splat cooled glass annealed at 725 °C for 500 h was investigated using TEM. The samples were prepared by the crushing method, where a few grams of glass were crushed into fine powder using an agate mortar. The resulting fine powder was then dispersed in pure ethyl alcohol medium in a 50 ml beaker by keeping the solution in an ultrasonic bath for few minutes. A carbon coated 200-mesh TEM copper grid was placed on a wire support inside the beaker. After some minutes suspension's particles had decanted on the grid, which was then removed from the beaker. Alcohol in the grid was evaporated by its own vapor pressure at room temperature, leaving the glass particles adhered to the grid surface.

3. Results

Fig. 1(a) shows a series of sequential Nyquist diagrams obtained during annealing a splat cooled sample at 400 °C ($T_g = 580$ °C). The sample's electrical resistance increase with time. Similar plots were found for other annealing temperatures below T_g.

As an example, Fig. 1(b) shows a series of sequential Nyquist diagrams obtained during annealing a splat cooled sample at 590 °C. There is a decrease of the sample's electrical resistance with time. Similar plots are found for other annealing temperatures above T_g.

The evolution of the electrical conductivity during annealing at different temperatures is shown in Fig. 2. For simplicity, relative variations of conductivity are plotted $\Delta\sigma = (\sigma(t) - \sigma(0))/\sigma(0)$, this allows one to work with a linear scale in the coordinate axis. Fig. 2 is originated from plots similar to those of Fig. 1, taking for each time, sample resistance as the intersection of the semicircle of the Nyquist diagram with the **x** axes. As in Fig. 1, annealing at temperatures *below* T_g displays a *decrease* in electrical conductivity, while *at or above* T_g an *increase* in σ is observed. In this case T_g refers to the homogeneous glass (before PS).

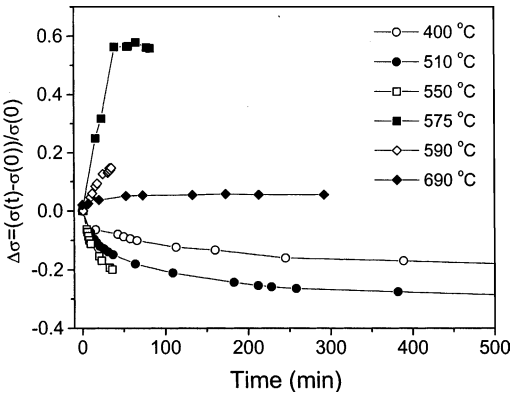

Fig. 2. Relative electrical conductivity evolution during annealing at different temperatures.

Fig. 3 shows Arrhenius plots for the 300–400 °C temperature range after annealing samples at the temperatures detailed in Section 2.2. Note that measurements were performed at temperatures below the annealing temperatures to keep unchanged the PS structures (that developed during the previous annealing treatments). From their

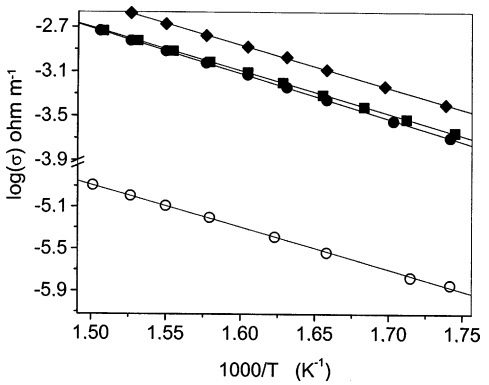

Fig. 3. Arrhenius plots of the glasses after annealing at 400 °C (open circles), 510 °C (solid circles), 580 °C (solid squares) and 690 °C (solid diamonds).

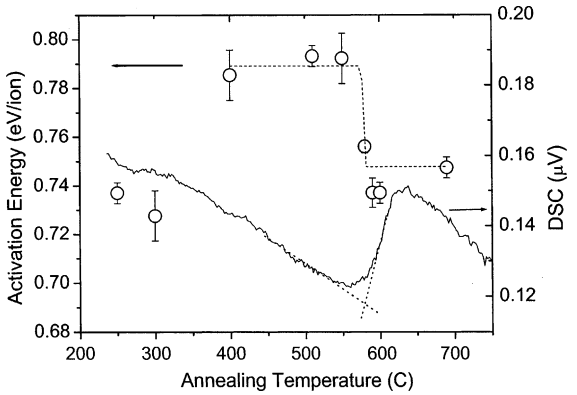

Fig. 4. E_a vs. annealing temperature: open circles: values obtained by impedance spectroscopy (dotted lines are used as guide lines). Full line: DSC run indicating the glass transition temperature T_g at 580 °C.

slopes, the activation energies for electrical conduction were calculated and are presented in Fig. 4 as a function of the previous annealing temperature. Fig. 4 also shows, overlapped with the activation energies, a DSC run indicating the glass transition temperature T_g at approximately 580 °C.

Additional information about the PS morphology is obtained by TEM. Glass samples splat cooled from 1600 °C to room temperature and observed by TEM showed a unique homogeneous phase and no evidence of liquid–liquid PS. However, Fig. 5(a) shows that after about 500 h of annealing at 725 °C, large particles – having tens of nanometers in diameter – appear inside a fine structure with dimensions of about 10 Å. The fine structure quickly develops during the first moments of annealing, and impedance spectroscopy detects the evolution of this structure. It was also possible to observe the fine structure on a splat-cooled sample after exposing it to the TEM electron beam for a few minutes. Fig. 5(b) shows the electron diffraction pattern corresponding to the bright field micrograph in Fig. 5(a). It displays the characteristic scattering halo of amorphous materials.

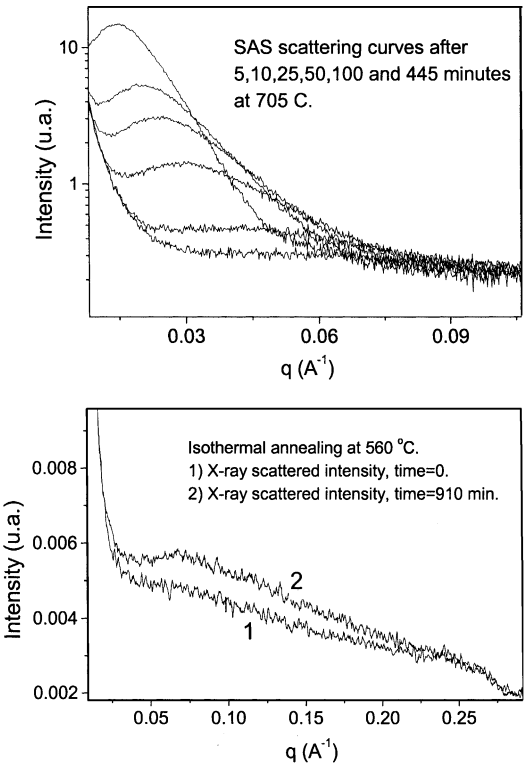

Fig. 6. (a) Sequence of in situ SAXS scattered intensity after 5, 10, 25, 50, 100 and 445 min (intensity increases with annealing time) at 705 °C, (b) at 560 °C.

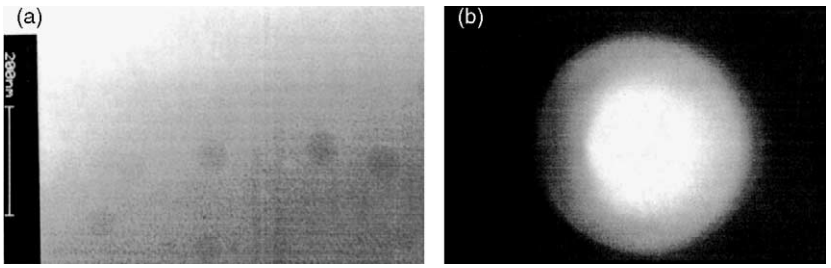

Fig. 5. (a) Fine and coarse amorphous particles after 500 h annealing at 725 °C; (b) electron diffraction pattern of the region in (a) showing halo corresponding to an amorphous structure.

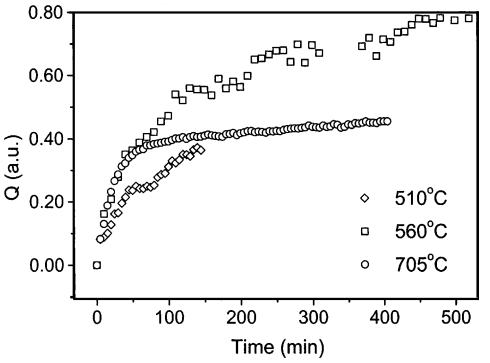

Fig. 7. Evolution of the invariant Q (see Eq. (2)) during annealing at different temperatures.

In situ SAXS measurements confirm the presence of phases having different electronic densities at least in the temperature range 510–705 °C, which includes T_g. Fig. 6 shows a strong increase of the scattered intensity with time and a shift of the maximum of the scattered intensity towards lower **q**. Fig. 7 shows the evolution of the Porod invariant Q, which monotonically increases with time for all the temperatures, below or above the glass transition temperature. Fig. 8 shows that WAXS could not detect crystalline phases for all heat treatments.

4. Discussion

Figs. 5(b) and 8 indicate the absence of crystalline phases during annealing. Moreover, the increase of the SAXS invariant Q in Fig. 7 denotes the existence of phases with different electronic densities, which evolve with time during annealing near T_g. TEM, SAXS and impedance spectroscopy show changes in the glass properties during annealing. However, each technique provides complementary information.

TEM shows that after short annealing times (a few minutes) fine size PS, with typical dimensions of about 10 Å takes place. Long time (longer than 100 h) annealing at 705 °C produces a similar fine structure, but a new phase of larger particles, having tens of nanometers in diameter (see Fig. 5(a)), also appears. The problem with TEM experiments is that the sample's temperature is not controlled during exposition to the electron beam. However, during SAXS, WAXS and impedance spectroscopy experiments, the heat dissipated by the X-ray beam or the electron current is negligible, thus the sample's temperature is easily controlled by a furnace.

The most interesting finding of this work is that the electrical conductivity shows a different behavior below and above T_g (of the quenched, single phase glass), during isothermal annealing. The electrical conductivity increases during annealing at temperatures at or above T_g, and decreases below T_g (Fig. 2). A cut in Fig. 2 at time = 25 min, shows the striking different behaviors below and above T_g (see Fig. 9). Moreover, there is an

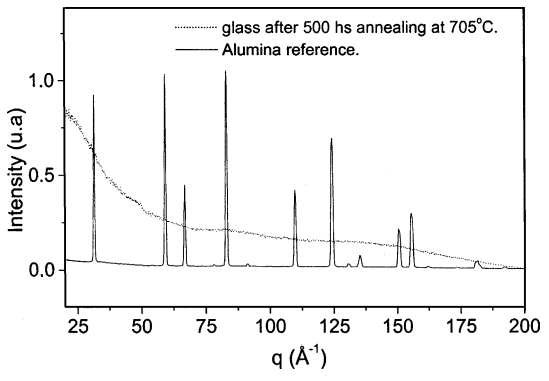

Fig. 8. WAXS of a glass sample after 500 h annealing at 705 °C. The peaks correspond to alumina used as a standard. No crystallization is observed after a long heat treatment.

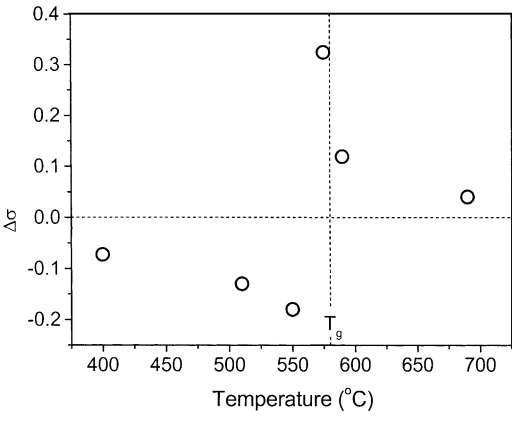

Fig. 9. Relative change in electrical conductivity, $\Delta\sigma$, after 25 min at different temperatures. T_g taken from Fig. 4 is also shown.

increase of about 5% of the activation energy of conductivity after annealing below T_g.

Do these different behaviors correspond to dissimilar processes? According to the SAXS results, below and above T_g, an increase of the Q invariant is observed with annealing time (Fig. 7), indicating an increase in the volume of the scattering phase or in the electronic density difference of the phases that appear during PS (Eq. (1)). Thus, both behaviors, increase and decrease of electrical conductivity, are due to liquid–liquid PS.

We should stress that we use T_g (of the quenched glass) just as a reference temperature because after PS the two glassy phases–silica rich and silica improverished (rich in Na_2O and B_2O_3)–probably have widely different T_g.

Electrical conduction in the present glass is mainly due to transport of Na ions. Since the electrical conductivity decreases with annealing time at temperatures below T_g this could mean that a sodium poor continuous phase is formed during these heat treatments, i.e., in the early stages of PS (see Fig. 7). However, above T_g, σ increases with time, indicating that a Na enriched continuous phase develops.

5. Conclusions

Impedance spectroscopy is very sensitive to detect slight structural changes in glasses, even at temperatures below T_g. In the glass studied here, the decrease of electrical conductivity and concomitant increase of the corresponding activation energy for annealing temperatures below T_g suggest that an interconnected SiO_2 rich matrix, with Na-rich islands is formed. This is ascribed to Na diffusion, since Si ions should not migrate at this temperature. The increase in electrical conductivity for treatments above T_g suggest the formation of an interconnected Na-rich phase.

TEM and SAXS experiments agree in that the characteristic size of particles is only a few nanometers. SAXS/WAXS experiments confirm that the electrical conductivity evolutions below and above T_g are due to PS. WAXS experiments did not detect any diffraction peak ascribable to crystalline phases during annealing.

Acknowledgements

The authors acknowledge LEG – DEMA – Universidade Federal de São Carlos, Brazil, for the use of the impedance analyzer, and to Vladimir Fokin, Luciana F. Maia and Ralf Keding for helpful discussions. Critical comments from Iria Polyakova were gratefully appreciated. We also acknowledge Tomás Plivelic and Iris Torriani for assistance with the SAXS measurements. This research has been partially granted by the Laboratório Nacional de Luz Sincrotrón, Campinas-Brazil, through project #963-2001, CNPq, Cyted, FAPESP (Brasil) and CONICET (Argentina).

References

[1] O.V. Mazurin, E.A. Porai-Koshits, Phase Separation in Glass, Elsevier, North-Holland, 1984.
[2] J. Rincon, A. Durán, Separación de fases en vidrios-El sistema Na_2O–B_2O_3–SiO_2, Monography of the Sociedad Española de Cerámica y Vidrio, Madrid, 1982.
[3] I.G. Polyakova, Phys. Chem. Glasses 41 (5) (2000) 247.
[4] C. Ravagnani, R. Keding, C. Rüssel, J. Non-Cryst. Solids 328 (2003) 164.
[5] J.A. Souza, R.F. Jardim, R. Muccillo, E.N.S. Muccillo, M.S. Torikachvili, J.J. Neumeier, J. Appl. Phys. 89, Part 1–2 (11) (2001) 6636.
[6] A.M. Bevilacqua, N.B. Messi de Bernasconi, D.O. Russo, M.A. Audero, M.E. Sterba, A.D. Heredia, J. Nucl. Mater. 229 (1996) 187.
[7] M.O. Prado, N.B. Messi, I.C. Torriani, T.S. Plivelic, A.M. Bevilacqua, M.A. Arribére, J. Non-Cryst. Solids 289 (1–3) (2001) 175.
[8] J.R. Macdonald, Impedance Spectroscopy, John Wiley, New York, 1987 (p. 205).
[9] O. Glatter, O. Kratky, Small Angle X-ray Scattering, Academic Press, New York, 1982.
[10] G. Kellerman, F. Vicentin, E. Tamura, M. Rocha, H. Tolentino, A. Barbosa, A. Craievich, I. Torriani, J. Appl. Cryst. 30 (1997) 880.